Published in final edited form as:
Biomaterials. 2009 July ; 30(20): 3359–3370. doi:10.1016/j.biomaterials.2009.03.015.

The Roles of Matrix Polymer Crystallinity and Hydroxyapatite Nanoparticles in Modulating Material Properties of Photo-crosslinked Composites and Bone Marrow Stromal Cell Responses

Shanfeng Wang[a], **Diederik H. R. Kempen**[b], **Michael J. Yaszemski**[b,c], and **Lichun Lu**[b,c,*]

[a] Department of Materials Science and Engineering, The University of Tennessee, Knoxville, TN 37996, United States

[b] Department of Orthopedic Surgery, Mayo Clinic College of Medicine, 200 First Street SW, Rochester, MN 55905, United States

[c] Department of Physiology and Biomedical Engineering, Mayo Clinic College of Medicine, 200 First Street SW, Rochester, MN 55905,United States

Abstract

Two poly(ε-caprolactone fumarate)s (PCLFs) with distinct physical properties have been employed to prepare nanocomposites with hydroxyapatite (HA) nanoparticles via photo-crosslinking. The two PCLFs are PCLF530 and PCLF2000, named after their precursor PCL diol molecular weight of 530 and 2000 $g.mol^{-1}$, respectively. Crosslinked PCLF530 is amorphous while crosslinked PCLF2000 is semi-crystalline with a melting temperature (T_m) of ~40 °C and a crystallinity of 40%. Consequently, the rheological and mechanical properties of crosslinked PCLF2000 are significantly greater than those of crosslinked PCLF530. Structural characterizations and physical properties of both series of crosslinked PCLF/HA nanocomposites with HA compositions of 0%, 5%, 10%, 20%, and 30% have been investigated. By adding HA nanoparticles, crosslinked PCLF530/HA nanocomposites demonstrate enhanced rheological and mechanical properties while the enhancement in compressive modulus is less prominent in crosslinked PCLF2000/HA nanocomposites. *In vitro* cell attachment and proliferation have been performed using rat bone marrow stromal cells (BMSCs) and correlated with the material properties. Cell attachment and proliferation on crosslinked PCLF530/HA nanocomposite disks have been enhanced strongly with increasing the HA composition. However, surface morphology and surface chemistry such as composition, hydrophilicity, and the capability of adsorbing protein cannot be used to interpret the cell responses on different samples. Instead, the role of surface stiffness in regulating cell responses can be supported by the correlation between the change in compressive modulus and BMSC proliferation on these two series of crosslinked PCLFs and PCLF/HA nanocomposites.

* Corresponding author. Tel: (507) 284-2267. Fax: (507) 284-5075. Lu.Lichun@mayo.edu.

Keywords

Polycaprolactone fumarate (PCLF); Hydroxyapatite (HA); Nanocomposite; Photo-crosslinking; Bone marrow stromal cell responses

1. Introduction

Biodegradable and crosslinkable poly(ε-caprolactone fumarate) (PCLF) has been synthesized in our laboratory via polycondensation of poly(ε-caprolactone) (PCL) diol and fumaryl chloride in the presence of potassium carbonate [1,2]. By varying the molecular weight of PCL diol, PCLFs with controllable physical properties can be obtained to meet the design requirements of both hard and soft tissue engineering scaffolds [1-4]. Previously, we have reported the structural characterizations and physical properties of both uncrosslinked and crosslinked PCLFs [1-4]. Two-dimensional (2D) disks and three-dimensional (3D) nerve conduits have been also fabricated from PCLFs via photo-crosslinking [3-5]. *In vitro* cell studies such as cytocompatibility, cell attachment and proliferation, and *in vivo* implantation using a rat sciatic nerve injury model have been conducted and the biological evaluations of crosslinked PCLFs have been correlated with their physical properties [3-5]. Crosslinked PCLFs have demonstrated excellent cell viability with various cell types such as human fetal osteoblast cells, rat bone marrow stromal cells (BMSCs), and rat Schwann cell precursor line (SPL201) cells [2,4,5]. Although their flexibility and toughness make them suitable for fabricating nerve conduits to guide peripheral nerve regeneration [4], the mechanical properties of crosslinked PCLFs are yet to be strengthened for being used as bone-tissue-engineering materials, especially when they are amorphous at body temperature.

Hydroxyapatite (HA), the major inorganic component of bone mineral, has been used for various biomedical applications such as implant coating because of its advantages such as excellent bioactivity, promotion of cellular function, and osteoconductivity [6]. Because HA nanoparticles are brittle and cannot be applied to the load-bearing sites directly, they are often used as physical fillers to enhance the mechanical properties and osteoconductivity of numerous polymers such as PCL, poly(L-lactide) (PLLA), poly(lactide-*co*-glycolide) (PLGA), and poly(methyl methacrylate) (PMMA) [6-18]. Besides being used as pre-made HA nanoparticles with polymer matrices, they can be also generated *in situ* during polymer precipitation or synthesis to improve the interface between fillers and matrix [6,19]. Compared with the above-mentioned matrix polymers with saturated backbones, crosslinkable or injectable polymeric biomaterials exemplified by PCLFs have many advantages because they can be injected and hardened *in situ* to fill tissue defects or fabricated into pre-formed scaffolds [20-22]. There only exist a few crosslinked nanocomposites based on HA nanoparticles and crosslinkable polymer matrices such as polypropylene fumarate (PPF) and polyanhydride [16,23-27]. In the crosslinked PPF/HA nanocomposites reported by us, the addition of HA nanoparticles did not improve the compressive modulus significantly possibly because crosslinked PPF was intrinsically very rigid [23]. Nevertheless, dramatically enhanced cell attachment and proliferation have been observed on the crosslinked PPF/HA nanocomposite disks cut from cylinders because the HA nanoparticles exposed on the disk surface greatly increased hydrophilicity and the capability of adsorbing protein from cell culture medium [23].

In this study, we present novel photo-crosslinked biodegradable and bioactive nanocomposites for orthopedic applications by incorporating HA nanoparticles with PCLF matrix. Two PCLFs, PCLF530 and 2000, synthesized from the PCL diol precursors with the nominal molecular weights of 530 and 2000 $g.mol^{-1}$ have been used. Because of its amorphous characteristics, crosslinked PCLF530 has much lower mechanical properties compared with crosslinked

PCLF2000 that has a higher crystallinity and a melting temperature (T_m) higher than the body temperature [3,4]. Thus the enhancement of HA nanoparticles in these two matrices is expected to differ significantly. Another focus of this study is on regulating cell responses using different PCLFs and their nanocomposites. Recently the mechanical properties of biomaterials have been revealed to be crucial in influencing cell responses [28-30]. For instance, we reported that SPL201 cell proliferation could be enhanced dramatically on the bare crosslinked PCLF2000 surface with higher crystallintiy and mechanical properties compared to crosslinked PCLF530 [4]. Using rat BMSCs, we will present *in vitro* cell attachment and proliferation on the crosslinked PCLFs and PCLF/HA nanocomposites. Through this study, we not only supply a series of crosslinkable polymer/HA nanocomposites for bone tissue engineering applications, but also use them as model polymeric systems to suggest the roles of matrix polymer crystallinity and HA nanoparticles in regulating material properties and cell responses without greatly modifying the materials' surface chemistry.

2. Materials and methods

2.1. Materials

All chemicals used in this study were purchased from Sigma-Aldrich Co. (Milwaukee, WI) unless noted otherwise. PCLF530 and PCLF2000 were synthesized in our laboratory as described in previous reports [1], having a weight-average molecular weight (M_w) of 6050 and 12900 g.mol^{-1}, and a number-average molecular weight (M_n) of 3520 and 7300 g.mol^{-1}, respectively. HA nano-particles (~100 × ~20 nm^2, length × width) were purchased from Berkeley Advanced Biomaterials (Berkeley, CA).

2.2. Photo-crosslinking of PCLF/HA nanocomposites

Photo-crosslinking was initiated with ultraviolet (UV) light (λ=315-380 nm) using a photoinitiator phenyl bis(2,4,6-trimethyl benzoyl) phosphine oxide (BAPO, IRGACURE 819^{TM}, Ciba Specialty Chemicals, Tarrytown, NY). Similar to the preparation of crosslinked PCLFs [3-5], 150 μL of BAPO/CH_2Cl_2 (300 mg/1.5 mL) solution was mixed with a slurry formed by 500 μL CH_2Cl_2 and 1.5 g of PCLF/HA with varied HA weight composition (ϕ_{HA}) of 0%, 5%, 10%, 20%, and 30%. Homogeneous PCLF/HA/BAPO/CH_2Cl_2 mixture was transferred into a mold formed by two glass plates (2.1 mm, thickness) and a Teflon spacer (0.37 mm, thickness). The filled mold was placed under UV light with a distance of ~7 cm from the lamp head for 30 min to allow crosslinking. Crosslinked PCLF/HA sheets were removed from the mold after cooled down to ambient temperature. Strips and disks with different dimensions cut from the sheets were extracted in acetone for two days and dried in vacuum for various experiments.

2.3. Gel fraction and swelling ratio measurements

Two crosslinked PCLF or PCLF/HA disks (5 × 0.34 mm^2, diameter × thickness) were immersed in excess CH_2Cl_2. After two days, the disks were taken out and weighed after blotted quickly to remove the attached solvent on the surfaces. The solvent adsorbed in the disks was subsequently evacuated and the dry disks were weighed. Based on the measured weights of the original (W_0), dry (W_d), and fully swollen (W_s) disks, their swelling ratios and gel fractions were calculated using the equations of $(W_s\text{-}W_d)/W_d\times100\%$ and $W_d/W_0\times100\%$, respectively.

2.4. Structural and thermal characterizations

Fourier Transform Infrared (FTIR) spectra of HA, crosslinked PCLFs and PCLF/HA nanocomposites were obtained on a Nicolet 550 FTIR spectrometer using a zinc selenide ATR crystal. The resolution of the instrument was specified as 4 cm^{-1} at a wavenumber of 1000 cm^{-1}. Differential Scanning Calorimetry (DSC) measurements were performed on a Q1000

differential scanning calorimeter (TA Instruments) in a nitrogen atmosphere. To keep the same thermal history, each sample was first heated from room temperature to 100 °C and cooled to −90 °C at a cooling rate of 5 °C/min. A subsequent heating run was performed from −90 to 100 °C at a heating rate of 10 °C/min. Thermogravimetric analysis (TGA) was done in flowing nitrogen at a heating rate of 20 °C/min using a Q500 thermal analyzer (TA Instruments).

In wide-angle x-ray diffraction (WAXD) measurements, HA nanoparticles, crosslinked PCLF and PCLF/HA disks were suspended and run in transmission mode. A Bruker AXS micro-diffractometer with copper radiation, an incident beam monochromater, and a GADDS multi-wire area detector was used for the wide angle tests. Two frames were collected, one at the Bragg angle 2θ=20° and one at 50° to cover a range of 5° to 65° for 2θ. Each frame was collected for 5 min. The data was then integrated and plotted as intensity vs. 2θ peaks were identified using Material Data Incorporated's JADE 7.0 software.

2.5. Microscopic observation

Morphology of HA nanoparticles in the crosslinked PCLF/HA disks was examined by a transmission electron microscope (TEM) (1200-EX II, JEOL Inc., Japan). The sample was placed into plastic capsules filled with resin, hardened into at 60 °C for 24 h, and sectioned with a glass knife as a thick block with a thickness of 0.6 μm. For TEM imaging, the block was trimmed down to the area of interest and then sectioned with a diamond knife to a thickness of 0.1 μm. All samples were viewed at 80 kV accelerating voltage. Surface morphologies of the crosslinked PCLF and PCLF/HA disks were examined by a cold-field emission scanning electron microscope (SEM) (S-4700, Hitachi Instruments Inc., Japan). In SEM imaging, the sample was mounted onto an aluminum stub, sputter coated with gold-palladium, and viewed at 3 kV accelerating voltage.

2.6. Rheological and mechanical measurements

Linear viscoelastic properties of crosslinked PCLF and PCLF/HA disks, including storage and loss moduli G′ and G″ as well as viscosity η as functions of frequency, were measured using an AR2000 rheometer (TA Instruments) in the frequency (ω) range of 0.5-100 rad/s and at 37 and 60 °C, sequentially. Rheological measurements were performed with a small strain (γ=0.01) using an 8 mm diameter parallel plate flow cell and a gap around 0.5 mm, depending on the thickness of polymer disk. Tensile and compressive properties of crosslinked PCLF and PCLF/HA specimens were implemented at room temperature by a dynamic mechanical analyzer (DMA2980, TA instruments). Five specimens were measured and averaged per sample. In tensile measurements, crosslinked PCLF and PCLF/HA strips (~30 × ~2 × ~0.4 mm^3, length × width × thickness) were pulled at a rate of 0.5 $N.min^{-1}$ up to a maximum static force of 18 N. In compression measurements, modulus was measured on small crosslinked PCLF and PCLF/HA disks (4.1 × 0.36 mm^2, diameter × thickness) at a compression rate of 2 $N.min^{-1}$ up to a maximum static force of 18 N.

2.7. Contact angle measurement and protein adsorption

A static Knuss Drop Shape Analysis (DSA) system, including a Knuss G10 contact angle measurement instrument and a data analyzing software version of 1.51.0.26, was used to evaluate the hydrophilicity of the crosslinked PCLF and PCLF/HA disks using water as the liquid phase. Approximately 1 μL of water (pH=7.0) was injected on the disk surface. Contact angle measurement was performed after a static time of 30 s. A tangent method and “Sessile Drop Fitting” in the software were applied to fit the drop shape and calculate the contact angle. For each composition, three disks were used and six data points were taken for mean and standard deviation calculation.

The procedure for determining the concentration of adsorbed protein was described earlier [5]. Pre-wetted polymer disks (11 × 0.37 mm^2, diameter × thickness) were placed in culture medium containing 10% fetal bovine serum (FBS) (Gibco, Invitrogen Corp., Carlsbad, CA) for 4 h at 37°C. Then these disks were transferred into 48-well plates (one disk per well) and 600 μL of phosphate buffer saline (PBS) was used to wash the polymer disks three times. Five minutes of gentle agitation was applied, and PBS was discarded after each wash. Two hundred forty microliters (240 μL) of 1% sodium dodecyl sulfate (SDS) solution was added to the wells for 1 h at room temperature. The SDS solution was collected in a plastic vial and new SDS solution was put into those wells for another 1 h. This procedure was repeated twice and all the SDS solution was collected in one plastic vial. The concentrations of protein in the collected SDS solutions were determined on a microplate reader (SpectraMax Plus 384, Molecular Devices, Sunnyvale, CA) using a MicroBCA protein assay kit (Pierce, Rockford, IL). Albumin in the kit was used to prepare solutions in SDS with eight known concentrations for constructing a standard curve.

2.8. In vitro bone marrow stromal cell attachment and proliferation

Rat bone marrow stromal cells (BMSCs) were used to evaluate the biocompatibility of crosslinked PCLFs and PCLF/HA nanocomposites for bone regeneration and to demonstrate the effects of PCLF intrinsic characteristics and ϕ_{HA} on cell responses. Cryopreserved rat BMSCs were thawed and plated on polystyrene flasks in medium containing 500 mL α-Eagle's minimum essential medium (Invitrogen Co.), 50 mL fetal calf serum, and 5 mL of Penn/strep antibiotics. After plating, the suspension was incubated for 12 h in a 5% CO_2, 95% relative humidity incubator at 37 °C. Crosslinked PCLF and PCLF/HA nanocomposite disks were sterilized in excess 70% ethanol solution overnight with shaking, dried in vacuum, and washed with PBS at least three times prior to use. The disks were fixed on the bottom of 48-well tissue culture plates using autoclave-sterilized inert silicon-based high temperature vacuum grease (Dow Corning, Midland, MI) to prevent them from floating in the culture medium. Cells were seeded onto the disk surfaces or control tissue culture polystyrene (TCPS) at a plating density of 15,000 cells/cm^2 with 300 μL culture medium. A colorimetric cell metabolic assay (CellTiter 96 Aqueous One Solution, Promega, Madison, WI) based on the MTS tetrazolium compound was performed. UV absorbance at 490 nm, which was correlated to the viable cell number, was measured using a microplate reader. Cell proliferation was assessed using the MTS assay for 7 days. After 1, 4, and 7 days, culture medium was removed from the wells and the disks were washed with PBS twice. Then the attached cells were fixed in paraformaldehyde (PFA) solution for 10 min, washed twice with PBS, and permeabilised with 0.2% Triton X-100. The cells were stained with rhodamine-phaloidin for 1 hr at 37 °C and DAPI at room temperature for photographing. The morphology of attached cells was observed and recorded by using an Axiovert 25 Zeiss light microscope (Carl Zeiss, Germany).

2.9. Statistical analysis

The data for cell proliferation were summarized and analyzed using a one-way analysis of variance (ANOVA) with significance level set at $p<0.05$.

3. Results and Discussion

3.1. Structural characterizations

HA nanoparticles formed a stable slurry with PCLF in CH_2Cl_2 for photo-crosslinking. Crosslinked PCLF530 disks are transparent while all crosslinked PCLF2000 and nanocomposite disks are homogenously white or ivory from naked eyes because of crystalline structure and the presence of HA inorganic particles. Fig. 1 shows the TEM images of crosslinked PCLF2000/HA 5% and 30% nanocomposites. Needle-like HA nanoparticles with an average length of ~100 nm and an average width of ~20 nm are evenly dispersed in the

crosslinked PCLF2000 matrix in both cross and horizontal sections, as demonstrated in (a-d) and (e, f), respectively. Other PCLF/HA nanocomposites demonstrate similar dispersion of HA nanoparticles in the matrices without forming significant aggregates.

Because PCLF530 has a higher density of crosslinkable segments than PCLF2000 [3,4], the gel fraction of crosslinked PCLF530 is as high as ~90% while it is 68% for crosslinked PCLF2000, as shown in Fig. 2a. After HA nanoparticles are added, crosslinked PCLF2000/HA nanocomposites have higher gel fractions because HA nanoparticles are insoluble in CH_2Cl_2. Since HA particles block the UV light from sufficiently initiating the crosslinking of PCLF2000 chains, the increment in the gel fraction is slightly lower for crosslinked PCLF2000/HA than the theoretical prediction based on the gel fraction for crosslinked PCLF2000 and ϕ_{HA}. PCLF530/HA nanocomposites even exhibit no clear increment in the gel fraction. Nevertheless, the substantial gel fractions in Fig. 2a for the crosslinked samples suggest that the photo-crosslinking of PCLF/HA nanocomposites was sufficiently efficient when the thickness was around 0.37 mm.

Crosslinked PCLFs and PCLF/HA nanocomposites swell in organic solvents such as CH_2Cl_2 and acetone. Because the precursor molecular weight is higher for PCLF2000, crosslinked PCLF2000's swelling ratio is over four times than that for crosslinked PCLF530. As demonstrated earlier [3], the swelling ratio of the crosslinked PCLF/HA decreases with the crosslinking degree, which can be controlled by the amount of photo-initiator per sample. As shown in Fig. 2b, the swelling ratio of the crosslinked PCLF/HA nanocomposites in CH_2Cl_2 decreases significantly with ϕ_{HA} because HA does not contribute to the swelling while it increases the material stiffness. Compared to the theoretical predictions for the swelling ratios based on the assumption that HA will not swell or dissolve in CH_2Cl_2, the experimental values are lower in both cases, especially in crosslinked PCLF2000/HA nanocomposites. It may suggest that HA nanoparticles could adsorb PCLF chains on the particle surface and limit them from swelling together with the PCL networks. It should be mentioned that the samples used in the rest of this study were soaked in acetone and then fully dried to remove all the unreacted polymer chains and other leachable components. Consequently, the compositions of these washed disks may slightly deviate from the feed compositions, which will be discussed in Fig. 5. Acetone was used in washing instead because polymer disks sometimes crack in CH_2Cl_2 due to the solvent's rapid penetration.

The crystalline structures of HA nanoparticles, crosslinked PCLFs and PCLF/HA nanocomposites are demonstrated in the WAXD patterns in Fig. 3. Before crosslinking, PCLF samples have the same diffraction peaks at 2θ=20.2, 21.4, 22.0, 23.7, and 30.0° as their precursor PCL diols, corresponding to *d*-spacings of 0.440, 0.415, 0.403, 0.375, and 0.295 nm, respectively [3,31,32]. After crosslinking, the diffraction peak at 2θ=22.0° is no longer prominent for crosslinked PCLFs. Crosslinked PCLF530 disks are also amorphous and transparent, demonstrated by a broad diffraction peak centered at 2θ=20.2° (*d*=0.440 nm) in Fig. 3. In contrast, crosslinked PCLF2000 is still crystalline and the patterns for it and its nanocomposites show characteristic diffraction peaks at 2θ=21.4, 23.7, and 30.0°. HA nanoparticles are typical crystalline structures with sharp diffraction peaks that can be assigned to different planes as marked in its pattern in Fig. 3, in agreement with JCPDS files for high temperature sintered HA [23,33]. The diffraction peaks for HA nanoparticles are all present in the crosslinked PCLF/HA nanocomposites. The intensity of the broad peak attributing to crosslinked PCLF530 decreases with increasing HA composition. Unlike *in situ* formation of HA crystals in the presence of polymer matrix [16,34], the intensities of all peaks for HA remain largely the same because the physical blending of pre-formed HA nanoparticles with crosslinkable PCLF matrix and photo-crosslinking of the blends do not change the crystalline structure of HA.

3.2. Thermal, rheological, and mechanical properties

The DSC curves and thermal properties of crosslinked PCLFs and PCLF/HA nanocomposites are shown in Fig. 4 and Table 1, respectively. In consistent with our earlier reports [3-5] and the WAXD patterns in Fig. 3, crosslinked PCLF530 and PCLF530/HA nanocomposites are all amorphous, showing only one glass transition temperature (T_g) at ~52 °C in the heating run. The presence of HA does not influence T_g discernibly at the compositions of HA up to 30%. For crystalline crosslinked PCLF2000, T_g is slightly lower than that for crosslinked PCLF530 because of a lower crosslinking density [3,4]. After the addition of HA nanoparticles into crosslinked PCLF2000 matrix, T_m determined in the heating run does not change significantly despite a weak increase from 39.7 to 41.1 °C. However, the heat of fusion ΔH_m and crystallinity χ_c determined in the heating run are comparably smaller for the crosslinked PCLF2000/HA nanocomposites with the HA compositions of 10%, 20%, and 30% than those with 0% and 5%, which implies that the crystallization of PCL segments might be constrained by the adsorption of HA nanoparticles. More evidently, the crystallization temperature (T_c) determined in the cooling run increases progressively with ϕ_{HA} from 7.4 °C for crosslinked PCLF2000 to 19.7 °C for crosslinked PCLF2000/HA 30%, indicating that HA nanoparticles may play as nucleation sites for PCL segments to be able to crystallize at a higher temperature when the nanocomposite was cooled down from the amorphous melt state.

Fig. 5 shows the TGA thermograms of HA, crosslinked PCLF and PCLF/HA nanocomposites. HA nanoparticles are stable without significant weight drop (less than 5%) at temperatures up to 700 °C while crosslinked PCLF has one thermal degradation step around 400 °C. The onset degradation temperature T_d is 360 and 383 °C for crosslinked PCLF530 and PCLF2000, respectively. As shown in Table 1, T_d increases slightly with the composition of HA, in agreement with the crosslinked PPF/HA nanocomposites reported by us previously [23]. The residue at 650 °C after the degradation of crosslinked PCLF/HA increases proportionally with the composition of HA. Given the weight fraction of residue for crosslinked PCLF, which is 3.8% for crosslinked PCLF530 and 1.5% for crosslinked PCLF2000, the weight fractions of residue for the crosslinked PPF/HA nanocomposites with various HA compositions can be predicted. The calculated values are 8.6%, 13.4%, 23.0%, and 32.7%, in satisfactory agreement with the experimental values of 7.3%, 13.2%, 22.1%, and 32.8% for the crosslinked PCLF530/HA nanocomposites with the HA compositions of 5%, 10%, 20%, and 30%, respectively. In contrast, the calculated values of 6.4%, 11.3%, 21.2%, and 31.0% for the crosslinked PCLF2000/HA nanocomposites are noticeably lower than the experimental results of 7.5%, 13.6%, 24.6%, and 37.5% in Fig. 5 because the measured disks were washed in acetone while the crosslinked PCLF2000/HA nanocomposites have relatively lower gel fractions than the crosslinked PCLF530/HA nanocomposites (see Fig. 2). TGA thermograms of original crosslinked PCLF2000/HA samples without being washed indeed have the residue amounts similar to the calculated values.

In order to demonstrate the pure filler effect of HA nanoparticles on rheological properties, the measurement temperatures of 37 and 60 °C were deliberately selected for performing dynamic oscillatory frequency sweep experiments on the crosslinked PCLF530/HA and PCLF2000/HA nanocomposites, respectively. The polymer matrices for both nanocomposites are amorphous and elastomeric at these temperatures, so there is no enhancement from the PCL crystallites. The results are shown in Fig. 6. In these two series of nanocomposites, G′ is always larger than G″ and independent of frequency, and η shows shear thinning behavior in the frequency range studied here, indicating typical characteristics of polymer networks [35]. G′, G″, and η all increase with adding HA nanoparticles and such increment is dramatic when the ϕ_{HA} is larger than 10%. As reported recently by us [3,4], crosslinked PCLF530 has a higher plateau modulus or shear modulus of 0.89 MPa determined from the curve for G′ than 0.13 MPa for crosslinked PCLF2000 at amorphous state because G′ is dependent on the molecular weight M_c between

two neighboring crosslinks while this M_c is decided by the molecular weight of PCL diol precursor [3-5,36]. As the result, crosslinked PCLF530/HA nanocomposites have higher values for G′, G″, and η when crosslinked PCLF2000/HA nanocomposites are amorphous at 60 °C in Fig. 6b. Because of their amorphous characteristics, crosslinked PCLF530/HA nanocompsites have similar G′, G″, and η at 25 or 60 °C. In contrast, when the measurement temperature is below crosslinked PCLF2000's T_m of ~40 °C, crosslinked PCLF2000 and its nanocomposites with HA have much higher mechanical and rheological properties than crosslinked PCLF530 and its nanocomposites because of the enhancement from the PCL crystallites. For instance, G′ of crosslinked PCLF2000/HA nanocomposite at the frequency of 5 rad/s increases from 12.1 MPa to 36.5 MPa and further to 54.2 MPa when ϕ_{HA} increases from 10% to 20% and 30% at 37 °C.

Table 2 lists both tensile and compressive moduli of the crosslinked PCLF/HA nanocomposites at room temperature. Clearly, crosslinked PCLF2000/HA nanocomposites are stiffer and stronger than crosslinked PCLF530/HA nanocomposites at the same ϕ_{HA} as indicated by significantly higher tensile and compressive moduli. As shown in Table 2, tensile modulus increases progressively with ϕ_{HA} from 3.3±0.4 MPa for crosslinked PCLF530 to 12.4±2.8 MPa for crosslinked PCLF530/HA 30% nanocomposites, and from 116±25 for crosslinked PCLF2000 to 667±75 MPa for crosslinked PCLF2000/HA 30% nanocomposites by a factor of 3.8 and 5.8, respectively. Besides the effect of HA nanoparticles, more solid and smoother surface morphology of the nanocompsites may also be an origin for their higher mechanical properties, as discussed later in Section 3.3 and Fig. 7. Tensile strength at break varies randomly between 0.58±0.20 to 1.54±0.27 MPa for crosslinked PCLF530/HA nanocomposites and between 7.45±0.79 to 9.49±0.63 MPa for crosslinked PCLF2000/HA nanocomposites. The tensile modulus and strength of crosslinked PCLF2000 and its nanocomposites with HA are comparable to those (50-500 MPa and 10-20 MPa) of cancellous bone [6]. Tensile strain at break decreases significantly from 38.1±4.1% and 107.0±96.1% for crosslinked PCLF530 and PCLF2000 to 13.6±2.8% and 2.1±0.5% for their nanocomposites with 30% HA nanoparticles, indicating the mechanical properties were significantly altered. However, only crosslinked PCLF530/HA nanocomposites demonstrate a significant increase in compressive modulus from 3.2±0.3 to 11.3±0.8 MPa when ϕ_{HA} increases from 0% to 30%, approaching the compressive modulus of crosslinked PCLF2000. Similar to crosslinked PPF/HA and PMMA/HA nanocomposites [23], crosslinked PCLF2000/HA nanocomposites do not show significant ϕ_{HA} dependence for the compressive modulus, which only slightly increases from 11.8±0.5 MPa for crosslinked PCLF2000 to 16.3±1.2 MPa for crosslinked PCLF2000/HA 20%. It can be attributed to the already high compressive modulus of the matrix and deserves further investigations.

3.3. Surface morphology and chemistry

As mentioned earlier in Fig. 2, the gel fractions for crosslinked PCLF530/HA nanocomposites are around 90% but lower than 80% for crosslinked PCLF2000/HA. By adding insoluble HA nanoparticles, the gel fraction increases and consequently different surface morphologies can be observed for different samples. For both crosslinked PCLF530 and PCLF2000, a rather rough surface can be seen in Figs. 7a, b, e, and f since the substantial soluble fraction, i.e. uncrosslinked PCLF, was extracted using acetone. Crosslinked PCLF/HA nanocomposites have smoother surfaces shown in Figs. 7c, d, g, and h because the greater gel fractions and smaller swelling ratios prevented surface erosion and fluctuation when the nanocomposite disks were soaked in acetone.

Many studies on polymer/HA nanocomposites or HA surface coating revealed that cell adhesion and proliferation could be enhanced significantly through the improved hydrophilicity and capability of adsorbing protein from the cell culture medium when

hydrophilic HA particles were exposed to cells or proteins directly [6,8,10,12]. Our earlier research on crosslinked PPF/HA nanocomposites demonstrated similar results when the nanocomposite cylinders were cut into disks for cell studies and HA nanoparticles embedded inside the cylinder were exposed on the disk surface [23]. In contrast, the fabrication method used in this study was dramatically different as the PCLF/HA nanocomposite disks were directly crosslinked between two glass plates. Therefore, the liquid phase in the PCLF/HA mixture covered the HA nanoparticles and the hydrophilic characteristics and topology of HA nanoparticles might not be able to take effect on the surfaces of crosslinked PCLF/HA disks. The dominant composition of PCLF on the surface of the crosslinked PCLF/HA nanocomposites can be confirmed by the FTIR spectra in Fig. 8. Only absorption peaks for crosslinked PCLF can be found on the surfaces of crosslinked PCLF/HA nanocomposite disks while there lack characteristic peaks for HA nanoparticles, such as hydroxyl (-OH) groups at 3400 cm^{-1}. Consistent with earlier reports on crosslinked PCLFs [3], no absorption peak for crosslinkable carbon-carbon double bonds (−C=C-) can be found around 1650 cm^{-1} in Fig. 8 because they were consumed completely in photo-crosslinking.

Besides surface composition, two additional characteristic parameters, surface hydrophobicity and the capability of adsorbing proteins from cell culture medium, have been determined and shown in Fig. 9. In Fig. 9a, both series of crosslinked PCLF/HA nanocomposites demonstrate only a weak increase in the water contact angle, meaning that the nanocomposites did not become more hydrophilic when HA nanoparticles were added. Different surface roughness may have a strong impact on the contact angle results although intrinsically amorphous crosslinked PCLF530 is more hydrophilic than semi-crystalline crosslinked PCLF2000. The weak increase in the water contact angle with increasing ϕ_{HA} can be reasonably attributed to the more solid and smoother surface as demonstrated in Fig. 7 without much change in surface composition. Consistent with our earlier results [4], crosslinked PCLF2000 and PCLF2000/HA nanocomposites are more hydrophobic and have a higher contact angle from 63° to 69°, compared with the values between 51° and 59° for crosslinked PCLF530 and its nanocomposites. Fig. 9b shows the capability of adsorbing protein from cell culture medium for both series of crosslinked PCLF/HA nanocomposites. There is a rough trend of decrease with increasing the HA composition in the nanocomposites, particularly in crosslinked PCLF2000/HA. It can be interpreted as the combined result of smaller surface area and higher hydrophobicity that discourages cell culture medium from spreading on the disk surface.

3.4. In vitro cell studies

Three major factors for biomaterials to influence cell responses are chemical, topological, and mechanical [30]. By adding HA nanoparticles in to the crosslinkable PCLF matrices, we have achieved different crosslinked nanocomposites with varied chemical, topological, and mechanical properties. Generally it is believed that a rough surface could supply more surface area for integrins or proteins on the cell membrane to attach and for cells to communicate with each other and proliferate [30]. Meanwhile, a surface hydrophilicity with a water contact angle around 50° is desirable for cells to attach and proliferate [30]. Recently, strong evidence using numerous polymeric systems demonstrates that stiffer surface of biomaterials will aid the flux of calcium ions though the cell membrane and regulate actin-myosin associated with the attaching sites [28,29,37]. Consequently, cell adhesion and proliferation could be enhanced significantly by strengthening polymer substrates [28,29]. In order to explore their bone-tissue-engineering applications, the bare surfaces of the crosslinked PCLF/HA nanocomposite disks without being treated with adhesive proteins were evaluated in terms of supporting rat BMSCs to attach and proliferate in one week. It should be noted that degradation of crosslinked PCLF matrix is negligible in the duration of one week and cell viability of crosslinked PCLFs is close to 100%, as reported recently by us [4,5].

BMSC morphology on crosslinked PCLF/HA nanocomposite disks at days 1, 4, and 7 post-seeding are demonstrated in Figs. 10a and b, which are consistent with the corresponding MTS absorption results in Fig. 10c. Previously we have revealed that the crosslinked PCLF2000 is more supportive in cell proliferation using SPL201 cells because crosslinked PCLF2000 with a higher crystallinity has a higher surface stiffness and roughness than crosslinked PCLF530 [4]. Similar results can be observed using BMSCs in this study. Crosslinked PCLF530 could not support BMSC attachment and proliferation at days 1, 4, and 7, as demonstrated by sparsely attached cells with a round phenotype. When HA nanoparticles were added into the crosslinked PCLF530 matrix, the mechanical properties were enhanced greatly as shown in Table 2. As shown in Fig. 10a, BMSCs attached much better on the crosslinked PCLF530/HA when ϕ_{HA} is 10% or above, by showing more attached cells with a spread-out phenotype. At day 7 post-seeding, confluent cell layers can be observed on the crosslinked PCLF/HA disks. For crosslinked PCLF2000 and PCLF2000/HA nanocomposites, no significant differences can be found and all the attached cells have spread-out phenotype with distinct actin stress fibers. Cell confluency can be observed over all the disks with PCLF2000 at day 7 post-seeding.

As mentioned earlier in Table 2, the compression modulus for crosslinked PCLF530 was enhanced by increasing the composition of HA whereas only a slight increase was for crosslinked PCLF2000. Having a higher hydrophobicity and a much stiffer surface with similar morphology and capability of adsorbing protein, crosslinked PCLF2000 supported BMSC adhesion and proliferation more efficiently than crosslinked PCLF530. Crosslinked PCLF2000/HA nanocomposites have smoother surfaces compared with crosslinked PCLF2000 because of higher gel fractions and less surface mobility in the step of sample purification, while the surface chemistry did not change much to benefit cell attachment and proliferation. The role of mechanical factor in regulating cell responses can be reflected in both crosslinked PCLFs and PCLF/HA nanocomposites, though the enhancement in mechanical properties has different origins of crystallinity or HA nanoparticles. Previous investigations on other polymer/HA nanocomposites also revealed significantly higher cell proliferation and differentiation, which were attributed to surface chemical or morphological factors such as greatly increased protein adsorption or more HA sites for cell anchorage [8,16-18]. In this study, however, these two factors can be ruled out as discussed earlier with Figs. 7-9.

In future studies, porous 3D polymer and nanocomposite scaffolds with pre-designed structures have been made using solid free-from fabrication methods [38,39]. Furthermore, PLGA microspheres containing human recombinant bone morphogenetic protein-2 (rhBMP-2) will be incorporated into PCLF/HA nanocomposite scaffolds with optimized structural features to induce bone formation and repair bone defects. As revealed in this study, the roles of matrix polymer crystallinity and HA nanoparticles are critical in modulating nanocomposites' physicochemical properties and regulating cell responses. The information on 2D cell-material interaction supplied in the present study will aid the understanding of 3D cell culture and *in vivo* animal implantations of porous bone scaffolds made from these crosslinkable or injectable polymers and nanocomposites [1-5,23,40,41].

4. Conclusions

Photo-crosslinked nanocomposites consisting of poly(ε-caprolactone fumarate) (PCLF) and hydroxyapatite (HA) nanoparticles have been prepared and extensively characterized in terms of crystalline structures, morphology, thermal, rheological, and mechanical properties. Two PCLFs with different precursor molecular weights and crystallinities demonstrate dramatically distinct mechanical properties and rat bone marrow stromal cell (BMSC) responses. Amorphous crosslinked PCLF530 with lower mechanical properties did not support cell attachment and proliferation while semi-crystalline crosslinked PCLF2000 with a higher hydrophobicity and much stiffer mechanical properties supported. Opposite to earlier studies

with substantial HA exposure on the surface, both crosslinked PCLF/HA nanocomposites demonstrated more hydrophobic and smoother surfaces with the lower capability for adsorbing protein upon adding HA nanoparticles to the polymer matrix. When the HA composition increases from 0% to 30%, tensile modulus increases by a factor of 3.8 and 5.8 for crosslinked PCLF530/HA and PCLF2000/HA nanocomposites, respectively. Softer crosslinked PCLF530 was enhanced greatly in compressive modulus with the addition of HA nanoparticles; however, stiffer crosslinked PCLF2000 did not increase significantly. Consequently, the role of compressive modulus can be found in regulating cell responses on the surfaces of two crosslinked PCLF/HA nanocomposites. Crosslinked PCLF530/HA nanocomposites exhibited enhanced rat BMSC attachment and proliferation. In contrast, no significant difference was found in crosslinked PCLF2000/HA nanocomposites when compared with crosslinked PCLF2000 as the polymer matrix is already favorable for BMSC attachment and proliferation. Besides supplying novel injectable polymers and nanocomposites with promising osteoconductivity for bone tissue engineering, this study suggests the role of enhancing BMSC attachment and proliferation through improving mechanical properties either by the crystalline domains or HA nanoparticles.

Acknowledgments

This work was supported by the Mayo Foundation and NIH (R01 AR45871 and R01 EB003060). DHRK thanks the Netherlands Organization for the support of Health Research and Development ZonMW (Agiko 920-03-325). The authors would like to thank James A. Gruetzmacher for assistance with polymer synthesis and characterization and Dr. Theresa E. Hefferan for providing BMSCs. We also thank Zhenqing Li at Clemson University for performing contact angle measurements. Wide-angle X-ray diffraction measurements were carried out in the Institute of Technology Characterization Facility, University of Minnesota, which receives partial support from NSF through the NNIN program.

References

1. Wang S, Lu L, Gruetzmacher JA, Currier BL, Yaszemski MJ. Synthesis and characterizations of biodegradable and crosslinkable poly(ε-caprolactone fumarate), poly(ethylene glycol fumarate), and their amphiphilic copolymer. Biomaterials 2006;27:832–41. [PubMed: 16102819]
2. Jabbari E, Wang S, Lu L, Gruetzmacher JA, Ameenuddin S, Hefferan TE, et al. Synthesis, material properties and biocompatibility of a novel self-crosslinkable poly(caprolactone fumarate) as an injectable tissue engineering scaffold. Biomacromolecules 2005;6:2503–11. [PubMed: 16153086]
3. Wang S, Yaszemski MJ, Gruetzmacher JA, Lu L. Photo-crosslinked poly(ε-caprolactone fumarate) networks: roles of crystallinity and crosslinking density in determining mechanical properties. Polymer 2008;49:5692–9.
4. Wang S, Yaszemski MJ, Knight AM, Gruetzmacher JA, Windebank AJ, Lu L. Photo-crosslinked poly (ε-caprolactone fumarate) networks for guided peripheral nerve regeneration: material properties and preliminary biological evaluations. Acta Biomater. 2009 in press.
5. Wang S, Kempen DH, Simha NK, Lewis JL, Windebank AJ, Yaszemski MJ, et al. Photo-cross-linked hybrid polymer networks consisting of poly(propylene fumarate) and poly(caprolactone fumarate): controlled physical properties and regulated bone and nerve cell responses. Biomacromolecules 2008;9:1229–41. [PubMed: 18307311]
6. Murugan R, Ramakrishna S. Development of nanocomposites for bone grafting. Compos Sci Technol 2005;65:2385–406.
7. Thomson RC, Yaszemski MJ, Powers JM, Mikos AG. Hydroxyapatite fiber reinforced poly(α-hydroxy ester) foams for bone regeneration. Biomaterials 1998;19:1935–43. [PubMed: 9863527]
8. Zhang R, Ma PX. Poly(α-hydroxyl acids)/hydroxyapatite porous composites for bone-tissue engineering. I. Preparation and morphology. J Biomed Mater Res 1999;44:446–55. [PubMed: 10397949]
9. Rizzi SC, Heath DJ, Coombes AGA, Bock N, Textor M, Downes S. Biodegradable polymer/hydroxyapatite composites: surface analysis and initial attachment of human osteoblasts. J Biomed Mater Res 2001;55:475–86. [PubMed: 11288075]

10. Wei G, Ma PX. Structure and properties of nano-hydroxyapatite/polymer composite scaffolds for bone tissue engineering. Biomaterials 2004;25:4749–57. [PubMed: 15120521]
11. Kim SS, Ahn KM, Park MS, Lee JH, Choi CY, Kim BS. A poly(lactide-*co*-glycolide)/hydroxyapatite composite scaffold with enhanced osteoconductivity. J Biomed Mater Res A 2007;80:206–15. [PubMed: 17072849]
12. Causa F, Netti PA, Ambrosio L, Ciapetti G, Baldini N, Pagani S, et al. Poly-ε-caprolactone/hydroxyapatite composites for bone regeneration: in vitro characterization and human osteoblast response. J Biomed Mater Res A 2006;76:151–62. [PubMed: 16258959]
13. Wiria FE, Leong KF, Chua CK, Liu Y. Poly-ε-caprolactone/hydroxyapatite for tissue engineering scaffold fabrication via selective laser sintering. Acta Biomater 2007;3:1–12. [PubMed: 17055789]
14. Wei J, Li Y. Tissue engineering scaffold material of nano-apatite crystals and polyamide composite. Eur Polym J 2004;40:509–15.
15. Moursi AM, Winnard AV, Winnard PL, Lannutti JJ, Seghi RR. Enhanced osteoblast response to a polymethylmethacrylate-hydroxyapatite composite. Biomaterials 2002;23:133–44. [PubMed: 11762831]
16. Opara TN, Dalby MJ, Harper EJ, Di Silvio L, Bonfield W. The effect of varying percentage hydroxyapatite in poly(ethylmethacrylate) bone cement on human osteoblast-like cells. J Mater Sci: Mater Med 2003;14:277–82. [PubMed: 15348475]
17. Dalby MJ, Di Silvio L, Harper EJ, Bonfield W. Increasing hydroxyapatite incorporation into poly (methylmethacrylate) cement increases osteoblast adhesion and response. Biomaterials 2002;23:569–76. [PubMed: 11761177]
18. Dalby MJ, Di Silvio L, Harper EJ, Bonfield W. Initial interaction of osteoblasts with the surface of a hydroxyapatite-poly(methylmethacrylate) cement. Biomaterials 2001;22:1739–47. [PubMed: 11396877]
19. Hakimimehr D, Liu DM, Troczynski T. In-situ preparation of poly(propylene fumarate)-hydroxyapatite composite. Biomaterials 2005;26:7297–303. [PubMed: 16026822]
20. Anseth KS, Shastri VR, Langer R. Photopolymerizable degradable polyanhydrides with osteocompatibility. Nature Biotech 1999;17:156–9.
21. Fisher JP, Dean D, Engel PS, Mikos AG. Photoinitiated polymerization of biomaterials. Annu Rev Mater Res 2001;31:171–181.
22. Ifkovits JL, Burdick JA. Photopolymerizable and degradable biomaterials for tissue engineering applications. Tissue Eng 2007;13:2369–95. [PubMed: 17658993]
23. Lee KW, Wang S, Yaszemski MJ, Lu L. Physical properties and cellular responses to crosslinkable poly(propylene fumarate)/hydroxyapatite nanocomposites. Biomaterials 2008;29:2839–48. [PubMed: 18403013]
24. Jayabalan M, Thomas V, Sreelatha PK. Studies on poly(propylene fumarate-co-ethylene glycol) based bone cement. Biomed Mater Eng 2000;10:57–71. [PubMed: 11086840]
25. Li H, Chen Y, Xie Y. Photo-crosslinking polymerization to prepare polyanhydride/needle-like hydroxyapatite biodegradable nanocomposite for orthopedic application. Mater Lett 2003;57:2848–54.
26. Li HY, Chen YF, Xie YS. Nanocomposites of crosslinking polyanhydrides and hydroxyapatite needles: mechanical and degradable properties. Mater Lett 2004;58:2819–23.
27. Hao J, Liu Y, Zhou S, Li Z, Deng X. Investigation of nanocomposites based on semi-interpenetrating network of [L-poly(ε-caprolactone)]/[net-poly(ε-caprolactone)] and hydroxyapatite nanocrystals. Biomaterials 2003;24:1531–9. [PubMed: 12559813]
28. Pelham RJ, Wang YL. Cell locomotion and focal adhesions are regulated by substrate flexibility. Proc Natl Acad Sci U S A 1997;94:13661–5. [PubMed: 9391082]
29. Discher DE, Janmey P, Wang YL. Tissue cells feel and respond to the stiffness of their substrate. Science 2005;310:1139–43. [PubMed: 16293750]
30. Harbers, GM.; Grainger, DW. 3 Cell-material interactions: fundamental design issues for tissue engineering and clinical considerations. In: Guelcher, SA.; Hollinger, JO., editors. An introduction to biomaterials. Boca Raton: CRC Press Taylor & Francis Group; 2006. p. 15-45.
31. Bittiger H, Marchess RH, Niegisch WD. Crystal structure of poly-ε-caprolactone. Acta Cryst 1970;B26:1923–7.

32. Lovinger AJ, Han BJ, Padden FJ Jr, Mirau PA. Morphology and properties of polycaprolactone-poly (dimethyl siloxane)-polycaprolactone triblock copolymers. J Polym Sci Part B Polym Phys 1993;31:115–23.
33. Rumpler M, Woesz A, Varga F, Manjubala I, Klaushofer K, Fratzl P. Three-dimensional growth behavior of osteoblasts on biomimetic hydroxyapatite scaffolds. J Biomed Mater Res A 2007;81:40–50. [PubMed: 17109410]
34. Chang MC, Ko CC, Douglas WH. Preparation of hydroxyapatite-gelatin nanocomposite. Biomaterials 2003;24:2853–62. [PubMed: 12742723]
35. Rubinstein, M.; Colby, RH. Polymer physics. New York: Oxford; 2003. p. 293
36. Sperling, LH. Introduction to physical polymer science. 3rd. New York: Wiley; 2001. p. 363-431.
37. Pelham RJ, Wang YL. Cell locomotion and focal adhesions are regulated by the mechanical properties of the substrate. Biol Bull 1998;194:348–9. [PubMed: 11536880]
38. Lee KW, Wang S, Lu L, Jabbari E, Currier BL, Yaszemski MJ. Fabrication and characterization of poly(propylene fumarate) scaffolds with controlled pore structures using three-dimensional printing and injection molding. Tissue Eng 2006;12:2801–11. [PubMed: 17518649]
39. Lee KW, Wang S, Fox B, Ritman EL, Yaszemski MJ, Lu L. Poly(propylene fumarate) bone tissue engineering scaffold fabrication using stereolithography: effects of resin formulations and laser parameters. Biomacromolecules 2007;8:1077–84. [PubMed: 17326677]
40. Wang S, Lu L, Gruetzmacher JA, Currier BL, Yaszemski MJ. A biodegradable and cross-linkable multiblock copolymer consisting of poly(propylene fumarate) and poly(ε-caprolactone): synthesis, characterization, and physical properties. Macromolecules 2005;38:7358–70.
41. Wang S, Lu L, Yaszemski MJ. Bone-tissue-engineering material poly(propylene fumarate): correlation between molecular weight, chain dimensions, and physical properties. Biomacromolecules 2006;7:1976–82. [PubMed: 16768422]

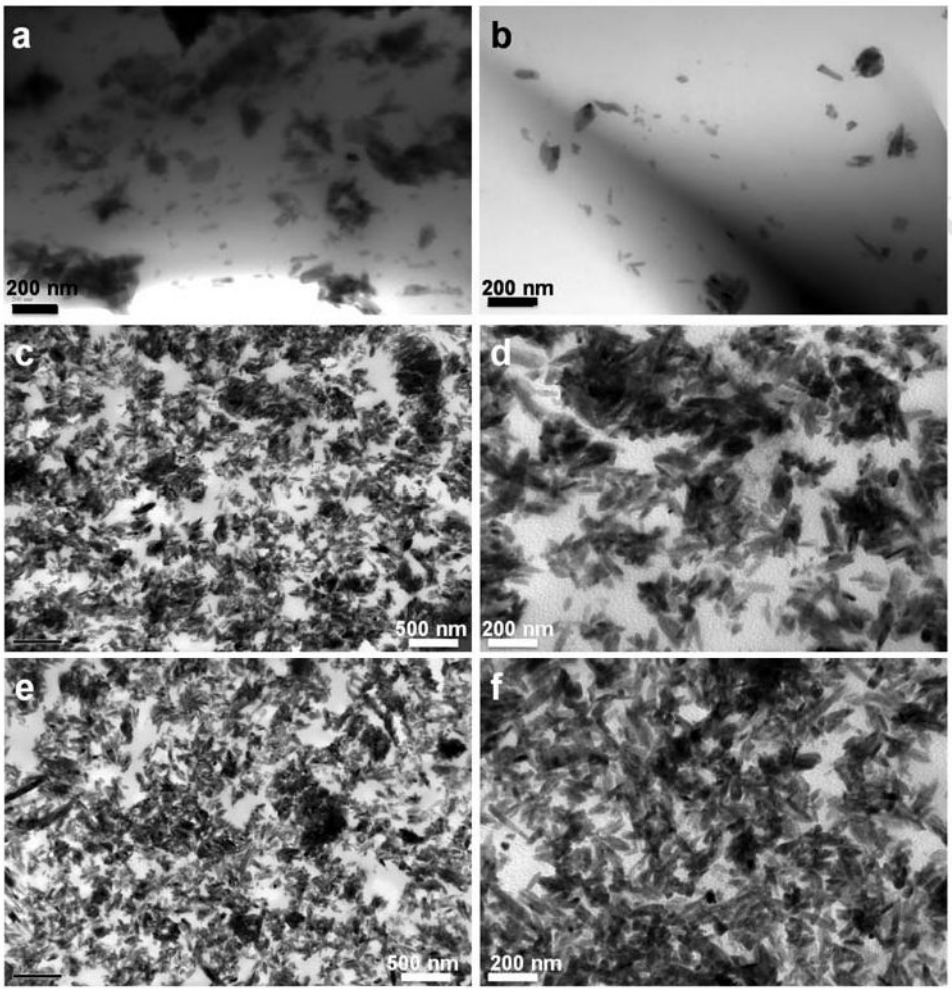

Fig. 1.

Transmission electron micrographs of the cross sections (a, b) of a crosslinked PCLF2000/HA 5% disk, and the cross section (c, d) and horizontal section (e, f) of a crosslinked PCLF2000/HA 30% disk. The images in d and f are magnified from the images in c and e, respectively. Scale bars represent 200 nm (a, b, d, f) and 500 nm (c, e).

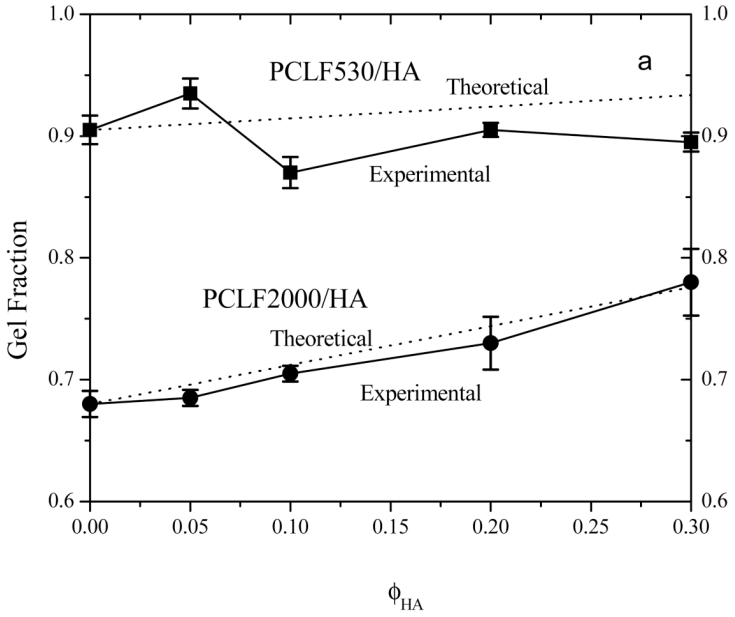

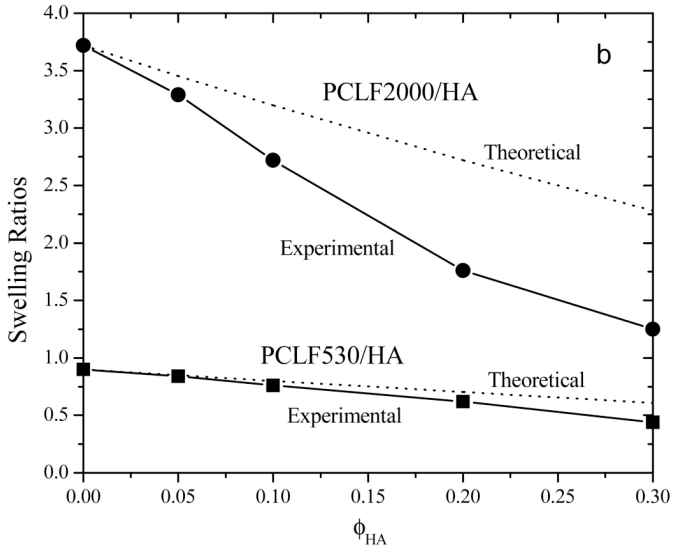

Fig. 2.

(a) Gel fractions of crosslinked PCLFs and PCLF/HA nanocomposites after being soaked in CH_2Cl_2 compared with the theoretical values marked as dotted lines, (b) swelling ratios of crosslinked PCLFs and PCLF/HA nanocomposites in CH_2Cl_2 compared with the theoretical values marked as dotted lines.

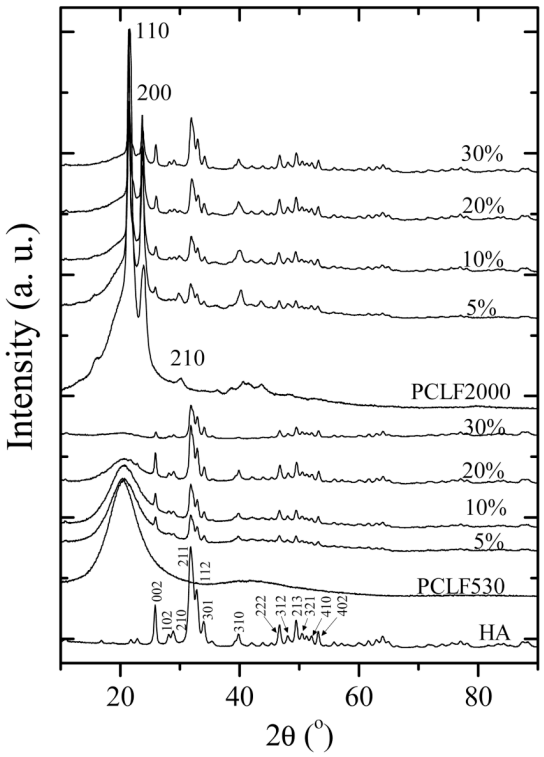

Fig. 3.

WAXD patterns of crosslinked PCLFs and PCLF/HA nanocomposites as well as pristine HA nanoparticles. HA peaks were indexed according to the JCPDS 9-432 standard. Three major peaks of crosslinked PCLF2000 were indexed horizontally.

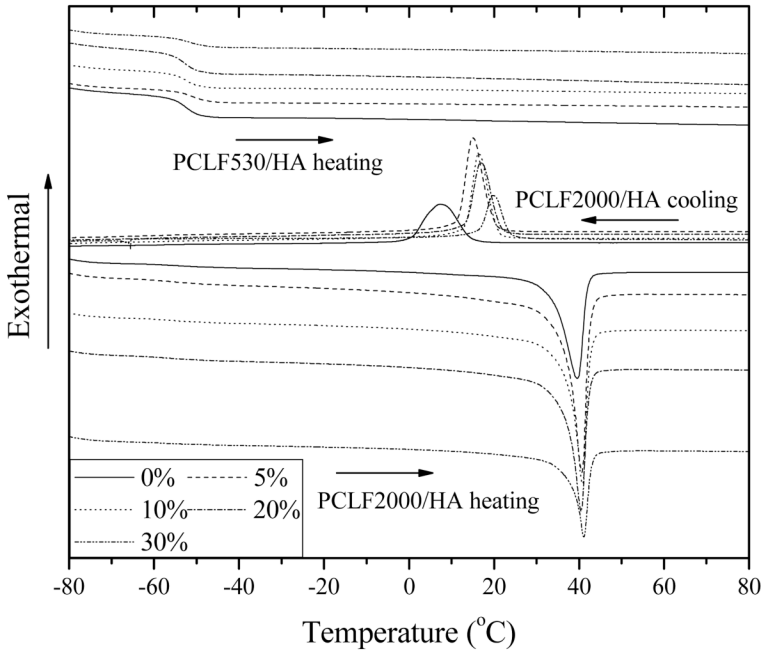

Fig. 4.
DSC curves of crosslinked PCLFs and PCLF/HA nanocomposites recorded in both cooling and heating runs with arrows to indicate the temperature change direction.

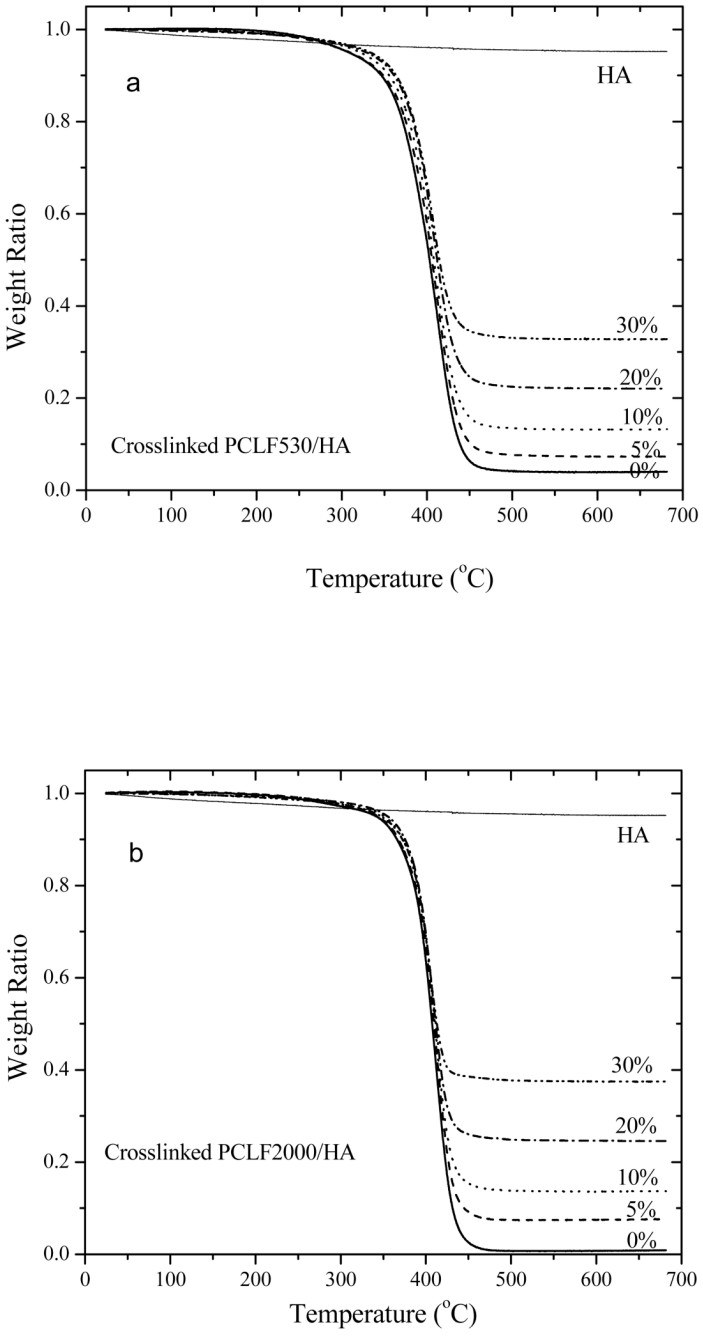

Fig. 5.
TGA thermograms of crosslinked PCLFs, PCLF/HA (a: PCLF530, b: PCLF2000) nanocomposites, and HA nanoparticles.

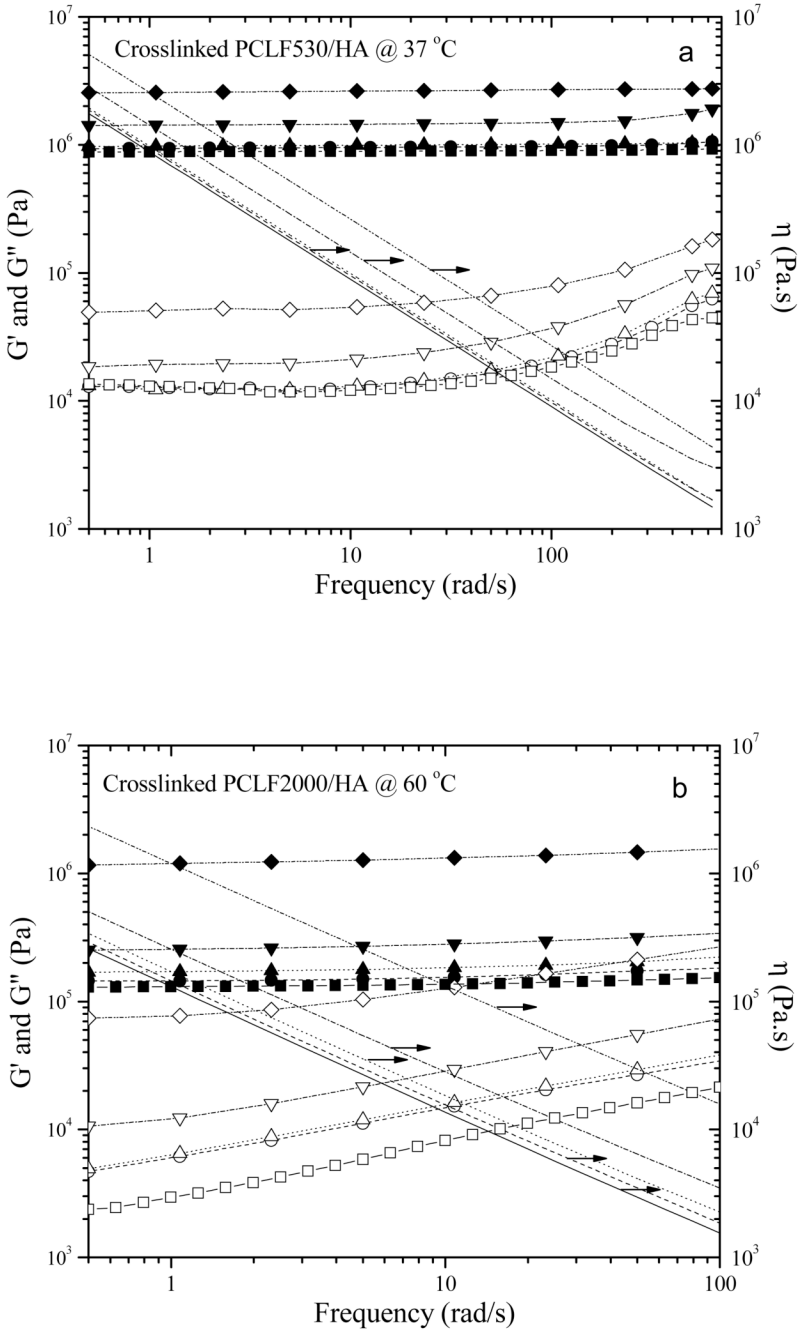

Fig. 6.

Storage modulus G′ (solid symbols), loss modulus G″ (open symbols), and viscosity η (lines) vs. frequency for (a) crosslinked PCLF530 and PCLF530/HA nanocomposites at 37 °C and (b) crosslinked PCLF2000 and PCLF2000/HA nanocomposites at 60 °C. Squares and/or solid lines, circles and/or dashed lines, upward-pointing triangles and/or dotted lines, downward-pointing triangles and/or dash-dotted lines, and diamonds and/or dash-double-dotted lines correspond to the HA composition of 0% to 30%, respectively.

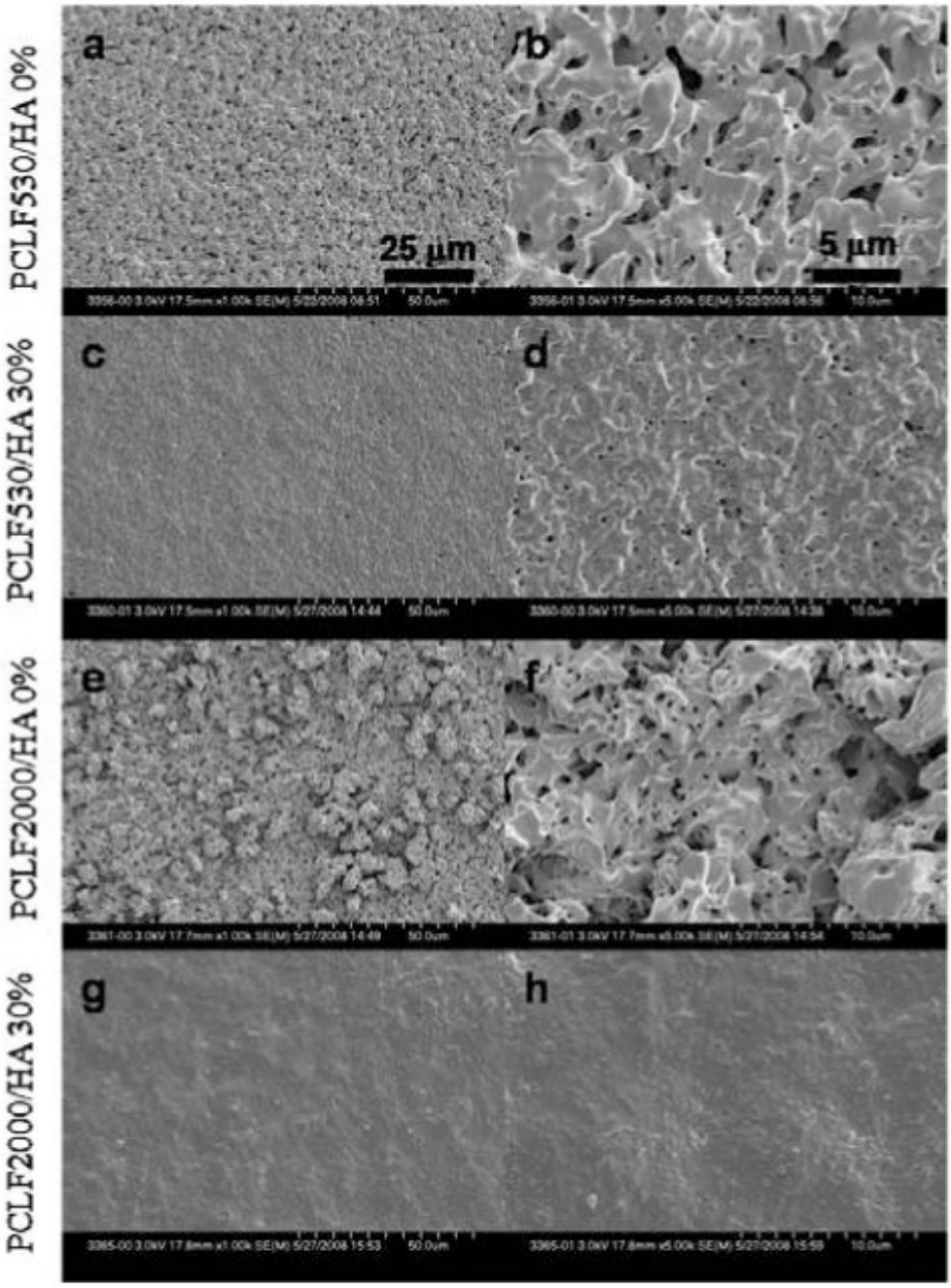

Fig. 7.

Scanning electron micrographs (a, c, e, g: ×1000, b, d, f, h: ×5000) of crosslinked disks of (a, b) PCLF530, (c, d) PCLF530/HA 30%, (e, f) PCLF2000, (g, h) PCLF2000/HA 30%. The images in b, d, f, and h are magnified from the images in a, c, e, and g, respectively. Scale bars represent 25 μm (a, c, e, g) and 5 μm (b, d, f, h).

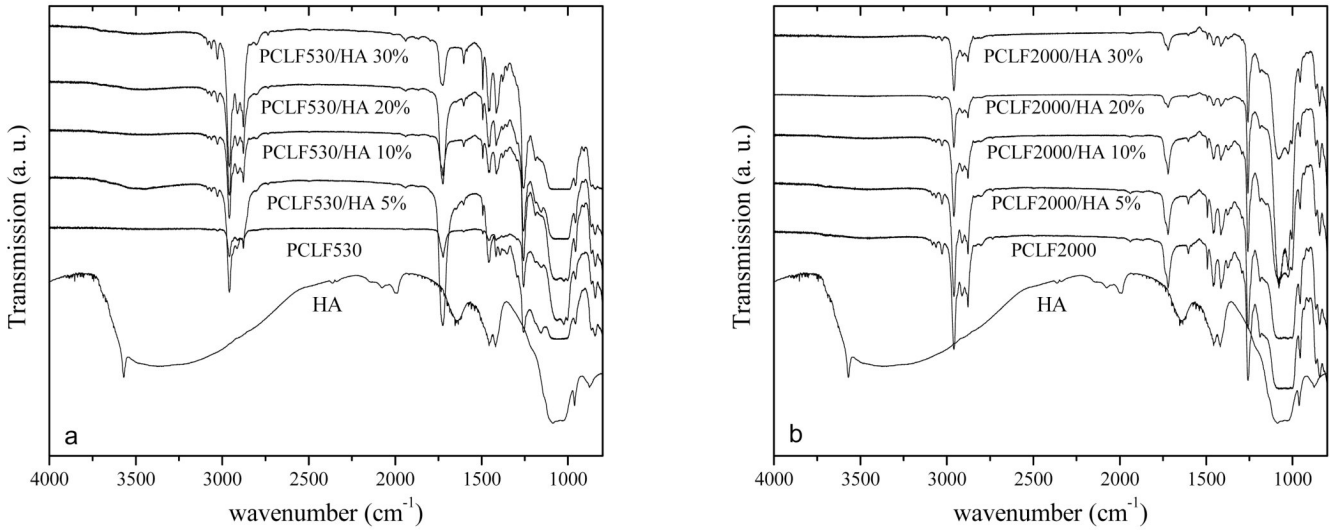

Fig. 8.
FTIR spectra of HA, crosslinked PCLFs and PCLF/HA (a: PCLF530, b: PCLF2000) nanocomposites.

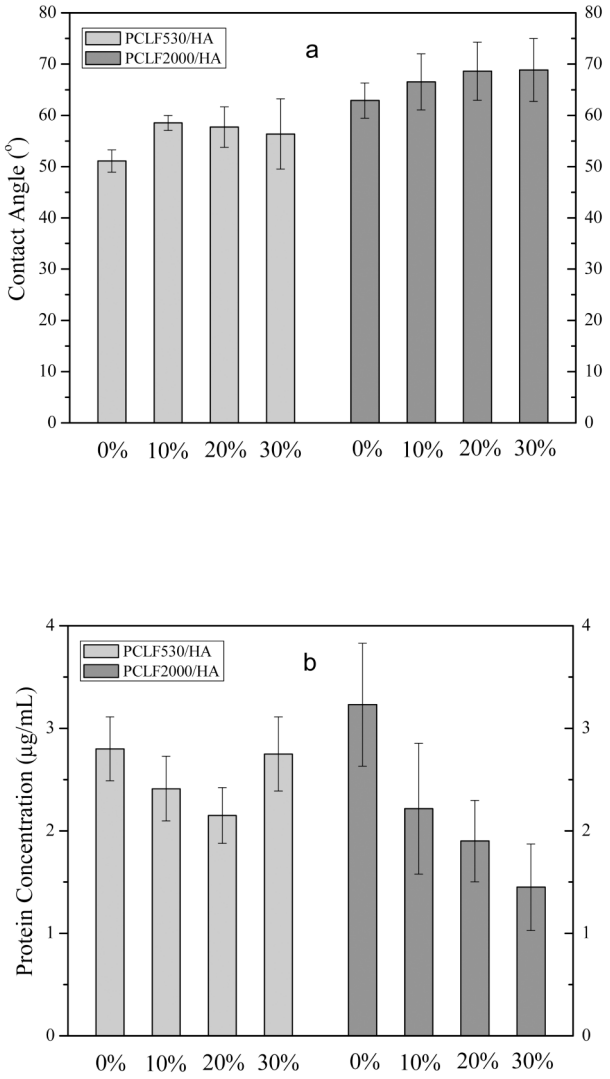

Fig. 9.

(a) Contact angles of water and (b) the concentrations of protein adsorbed on crosslinked PCLF and PCLF/HA nanocomposite disks.

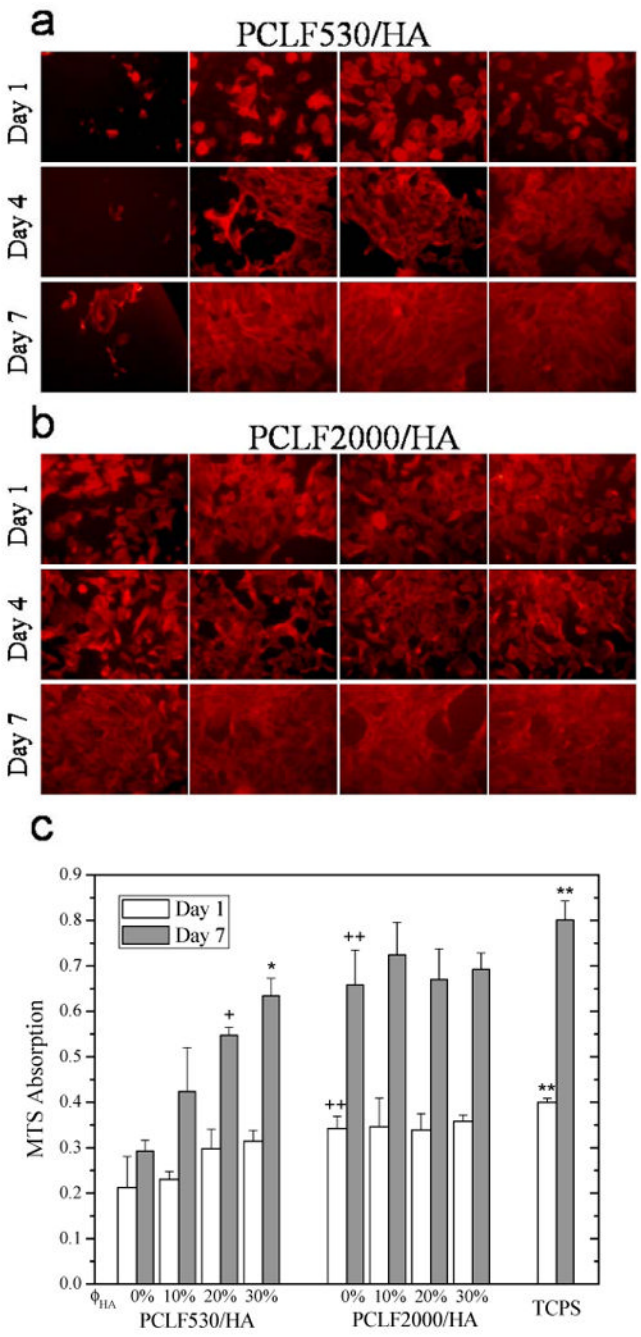

Fig. 10.

Morphology (×200) of rat bone marrow stromal cells on crosslinked PCLF and PCLF/HA nanocomposite (A: PCLF530, B: PCLF2000) disks 1, 4, and 7 days post-seeding. The scale bar of 200 μm in (a) is applicable to all. C: MTS absorption of bone marrow stromal cells on the disks of crosslinked PCLFs and PCLF/HA nanocomposites compared to cell-seeded tissue culture polystyrene (TCPS) as positive control. + $p<0.05$ between crosslinked PCLF530/HA 20% and 0% at day 7. * $p<0.05$ between crosslinked PCLF530/HA 30% and 0%, 10% at day 7. ++ $p<0.05$ between crosslinked PCLF2000 and PCLF530 at days 1 and 7. ** $p<0.05$ between TCPS and crosslinked PCLF2000, PCLF530 at days 1 and 7.

Table 1

Thermal properties of crosslinked PCLFs and PCLF/HA nanocomposites

	T_g (°C)	T_m (°C)	ΔH_m (J/g)	T_c (°C)	ΔH_c (J/g)	χ_c	T_d (°C)
PCLF530/HA 0%	-52.5 (-54.7)[a]	-	0	-	0	0	360
PCLF530/HA 5%	-51.5 (-54.7)[a]	-	0	-	0	0	370
PCLF530/HA 10%	-52.3 (-55.5)[a]	-	0	-	0	0	372
PCLF530/HA 20%	-52.9 (-55.5)[a]	-	0	-	0	0	374
PCLF530/HA 30%	-51.5 (-55.1)[a]	-	0	-	0	0	373
PCLF2000/HA 0%	-56.5	39.7	37.0	7.4	39.9	0.28[b]	383
PCLF2000/HA 5%	-55.0	40.7	33.0	14.9	33.0	0.26[b]	385
PCLF2000/HA 10%	-57.7	40.8	15.5	16.3	15.9	0.13[b]	385
PCLF2000/HA 20%	-57.7	40.5	18.0	16.8	21.3	0.17[b]	384
PCLF2000/HA 30%	-58.6	41.1	20.0	19.7	19.5	0.22[b]	381

[a] T_g out of or in parenthesis was determined in the heating or cooling run of DSC, respectively.

[b] The crystallinity of PCL in the crosslinked samples, χ_c, was calculated using the equation of $\chi_c=[\Delta H_m/(\phi_{PCL}\Delta H_m^c)]\times100\%$, where ΔH_m^c of PCL is 135 J/g and ϕ_{PCL} is $(1-\phi_{HA})\times98.1\%$ for crosslinked PCLF2000 and its nanocomposites.[1,3]

Table 2

Mechanical properties of crosslinked PCLFs and PCLF/HA nanocomposites

	Tensile Modulus (MPa)	Tensile Strength at Break (MPa)	Tensile Strain at Break (%)	Compressive Modulus (MPa)
PCLF530/HA 0%	3.31±0.41	1.04±0.19	38.1±4.1	3.18±0.31
PCLF530/HA 5%	4.22±0.05	0.58±0.20	14.3±5.2	4.34±0.22
PCLF530/HA 10%	5.37±0.59	0.68±0.16	13.9±3.9	6.41±0.81
PCLF530/HA 20%	6.82±0.89	1.24±0.43	19.3±6.5	7.27±0.85
PCLF530/HA 30%	12.4±2.76	1.54±0.27	13.6±2.8	11.3±0.77
PCLF2000/HA 0%	115.5±24.8	7.46±0.80	107.0±96.1	11.8±0.53
PCLF2000/HA 5%	237.7±22.5	9.49±0.63	12.8±2.8	14.5±1.23
PCLF2000/HA 10%	295.3±23.4	8.85±0.40	9.7±4.4	13.5±1.31
PCLF2000/HA 20%	444.9±52.2	8.52±0.98	4.2±1.1	16.3±1.23
PCLF2000/HA 30%	667.0±74.5	7.73±1.22	2.1±0.5	14.5±0.77